2014 IEEE International Conference on Robotics & Automation (ICRA)
Hong Kong Convention and Exhibition Center
May 31 - June 7, 2014. Hong Kong, China

Energy-efficient Propulsion Inspired by Whirligig Beetles

Xinghua Jia, Zongyao Chen, Andrew Riedel, William R. Hamel, *Fellow, IEEE,* and Mingjun Zhang*, *Senior Member, IEEE*

Abstract - **Whirligig beetle, claimed in the literature to be one of the highest measured for a thrust-generating apparatus within the animal kingdom, has evolved a series of propulsion strategies that may serve as a source of inspiration for designing highly efficient propulsive systems. First, a robotic platform was developed to test an energy-efficient propulsion mechanism inspired by the whirligig beetle. Second, a mathematical model for the robot was proposed to account for the fluid dynamics generated by the robotic swimming. Third, an optimal problem was formulated and solved for the propulsor and beating pattern design. The results indicated that soft middle, stiff end propulsor, and alternating, asymmetrical beating pattern will improve the propulsion efficiency for a swimming robot with four propulsors. Finally, simulation and experiments were conducted to further analyze the effect of beating pattern to the robotic propulsion efficiency. It was found that the oscillated body movement and *S*-shaped trajectory introduced by the optimal beating pattern would improve the propulsion efficiency for the designed robot.**

Ⅰ. INTRODUCTION

Walking, flying, and swimming animals have long been an important source of inspiration for robotics[1]. What makes the swimming organisms a unique source for bio-inspiration is their effective propulsive mechanisms [2, 3]. In this paper, we will propose an energy-efficient propulsion mechanism inspired by whirligig beetles, which were claimed in the literature to possess one of the most efficient thrust-generating apparatus within the animal kingdom [4]. Our group first discovered that the whirligig beetles' curved swimming trajectories gained energy efficiency over linear trajectories by alternating the ways the propulsors propelled [5]. Previous studies have concluded that whirligig beetles can swim at speeds of up to 44.5 body lengths/s with a maximum turning rate of 4428°/s and a maximum centripetal acceleration of 2.86 g [6]. In addition to the incredible speed, the insect is able to achieve a turning radius as small as 24% of the body length, and typically 84% of energy devoted to swimming can be transformed into forward propulsion [7, 8]. Additionally, it has been found that whirligig beetles are able to attain high swimming speeds, while reducing drag due to their unique propulsor structures, morphology, and beating patterns [7, 9].

This work was supported by the Office of Naval Research Young Investigator Program award (ONR-N00014-11-1-0622).

X. Jia, Z. Chen and W. R. Hamel are with the Department of Mechanical, Aerospace and Biomedical Engineering, The University of Tennessee, Knoxville, TN 37996 USA (e-mail: xjia8@utk.edu, zchen25@utk.edu, and whamel@utk.edu).

A. Riedel is with Department of Electrical Engineering and Computer Science, The University of Tennessee, Knoxville, TN 37996 USA (e-mail: ariedel@utk.edu).

M. Zhang was with the Department of Mechanical, Aerospace and Biomedical Engineering, The University of Tennessee, Knoxville, TN 37996 USA. He is now with the Departments of Biomedical Engineering and Internal Medicine, and the Dorothy M. Davis Heart & Lung Research Institute, The Ohio State University, Columbus, OH 43210 USA (e-mail: zhang.4882@osu.edu).

This paper will focus on bioinspired propulsor design and optimal beating pattern regulation to achieve efficient propulsion. To achieve these objectives, two optimization approaches for developing an energy-efficient propulsor and beating patterns were proposed and validated using a robotic platform designed and fabricated in our lab. A compliant propulsor with flexural rigidity determined by the stroke direction was proposed to realize a large area ratio between the power and recovery stroke and efficient utilization of fluid force. Finally, an energy efficient propulsion method was identified through beating pattern optimization and validated through simulation and experimental studies.

Ⅱ. BIOINSPIRATION FOR ENERGYEFFICIENT PROPULSION

A. Inspiration from the Whirligig Beetle

Three significant morphological characteristics of the whirligig beetle related to its propulsion efficiency are (a) propulsor's joint active actuation, (b) moving hairs, and (c) beating pattern regulation [5].

1) Micro/Nano-scale Morphologies of the Whirligig Beetle Propulsor

Through changing the propulsor's joint angles, whirligig beetles are able to control the propulsion and increase thrust. Fig.1(a) shows multiple joints, which are actuated to reach the desired positions for greater utilization of fluid force [4]. Based on this observation, we proposed a passively oscillated propulsor design actuated proximally. With proper flexural rigidity along the propulsor, it is feasible to regulate the compliant propulsor as the whirligig beetle does, and produced more thrust with the given actuation.

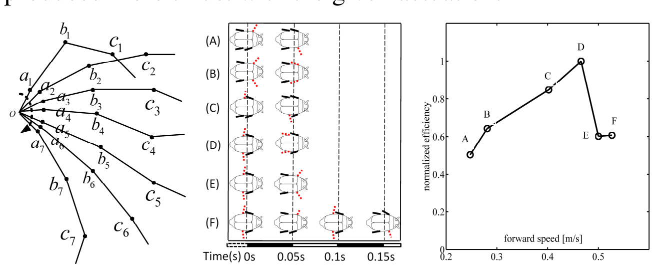

(a) (b) (c)

Fig. 1 (a) Trajectory of the right hind propulsor of whirligig beetle in power stroke (modified from [4]); (b) Six beating patterns used for forward swimming; (c) Normalized efficiency for the six beating patterns in (a). Efficiency was defined as: travelled distance/number of stroke.

Additionally, the moving hairs attached to the whirligig beetle propulsors increases the contact area with the fluid and allow a larger thrust [10]. Inspired from this, we designed a propulsor with stiff and soft flexural rigidity for the power and recovery stroke sides, respectively [11].

2) Propulsor's Beating Patterns

Whirligig beetles are able to regulate the beating of their propulsors in different situations to achieve high swimming efficiency [7]. Six beating patterns were selected [5, 7], and quantitatively analyzed for an efficient propulsion method development. With the results plotted in Fig.1 (c), we found the synchronized (Fig.1(b)-*Pattern D*) and alternating (Fig.1(b)-*Pattern C*) beating of the hind propulsors were more efficient than the others. Based on this observation, we proposed an optimization method to determine an energy efficient beating pattern.

B. Whirligig Beetle Inspired Swimming Robot

Inspired by the energy-efficient propulsion system of the whirligig beetle, we have developed a robotic platform (Fig.2) to realize efficient swimming. Dimensions of the robot body were scaled up proportionally about 35 times from the whirligig beetle. Propulsors were fabricated with flexible material and independently actuated by Hitec HS-5086WP waterproof servo motors. The servos can rotate at a speed of 60°/0.15s when powered by a TENERGY 6V/2000mAh battery. The mbed NXP LPC1768 microcontroller is connected to a laptop by a Bluetooth radio. In addition, acceleration, orientation and energy consumption are monitored real-time by a MPU-9150 and a custom power monitoring circuit. All the components are mounted on the custom designed PCB, and the total weight of the assembled robot is 817 g.

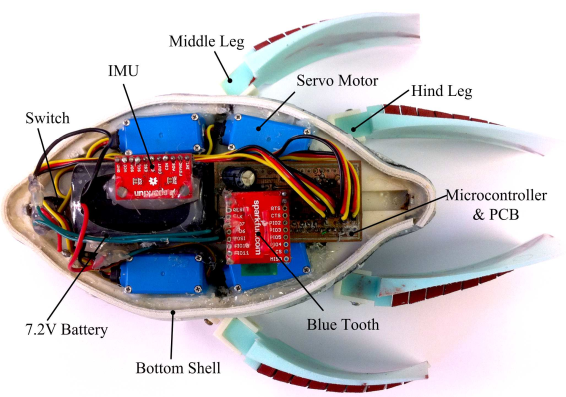

Fig. 2 Whirligig beetle inspired swimming robot. The robot shell was fabricated by a STRATASYS FORTUS 250mc 3D printer.

III.DYNAMICS MODELING OF PROPULSOR-BODY-FLUID INTERACTIONS AND DESIGN OPTIMIZATION OF EFFICIENT PROPULSION

Based on the whirligig beetle inspired swimming robot in *Section II-C*, a kinematics model of ellipsoid body with four chains was proposed to approximate the robotic locomotion. Fig.3 (b) shows the robot body parameters. The half axis lengths for the robot body are a_x, a_y, the moment of inertia is J_b, and the mass is M_b. In the global frame, the body mass center coordinates are $\Phi_b := [x_b \quad y_b]^T$, the orientation is θ_b and the k-th propulsor attaching point is $[x_0^k \quad y_0^k]^T$.

Fig.3 (c) shows parameters used to formulate the chain-link model for the k-th compliant propulsor. Divided into N links, each has length, mass, orientation, and moment of inertia of $l_i^k, m_i^k, \vartheta_i^k, J_i^k$ respectively; the actuation torque and elastic moment are denoted as u_i^k, $u_{E_i}^k$; $h_{x_i}^k$, $h_{y_i}^k$ are the internal force applied on the link ends; the fluid forces $f_{x_i}^k$, $f_{y_i}^k$ are applied on the mass center $[x_i^k \quad y_i^k]^T$; $s_{t_i}^k$, $s_{n_i}^k$ are the areas in the tangential and normal directions. The N-dimension vectors for the assembled links on the k-th propulsor are denoted as:

$$l^k, m^k, \vartheta^k, J^k, u^k, u_E^k, h_x^k, h_y^k, f_x^k, f_y^k, [x^k \quad y^k]^T, s_t^k, s_n^k.$$

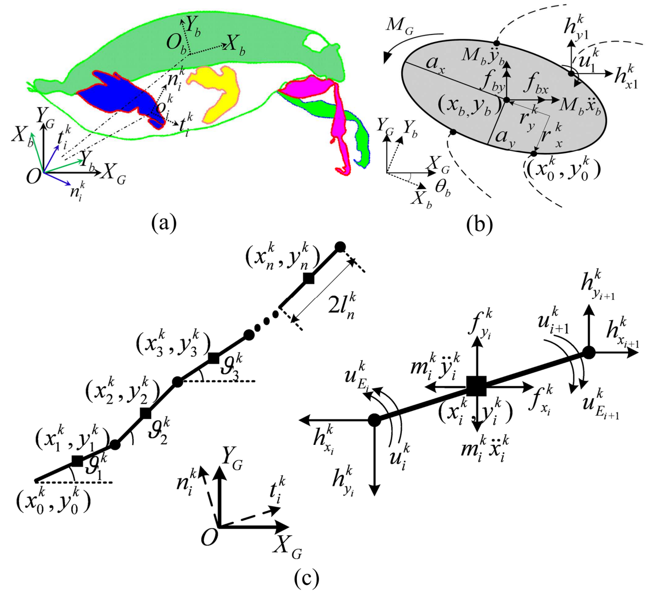

Fig.3 (a) Whirligig beetle robot coordinates systems, $O_G - X_G Y_G$ (global frame), $O_b - X_b Y_b$ (body frame), and O_i^k - $t_i^k n_i^k$, (k=1,2,3,4; i=1,2,...,N.) (propulsor link frame) (b) Whirligig beetle robot body model; (c) Chain link model for the compliant propulsor.

A. Propulsor Flexural Rigidity Optimization

In order to realize the propulsor flexural rigidity optimization, the propulsor was isolated from the body (superscript k used to distinguish propulsors can be neglected for all variables in *Section III-A*) and the flexural rigidity on the power stroke side was set large enough to guarantee thrust production. On the recovery stroke side, the flexural rigidity was set as $\kappa_1, \kappa_2, ..., \kappa_N$ for optimization.

1) Compliant Propulsor Model

By balancing the force and moment applied by the fluid and neighboring links (Fig.3(c)), the dynamics model for the propulsor is given as:

$$\begin{bmatrix} f_x \\ f_y \end{bmatrix} - m \begin{bmatrix} \ddot{x} \\ \ddot{y} \end{bmatrix} + \begin{bmatrix} B & \\ & B \end{bmatrix} \begin{bmatrix} h_x \\ h_y \end{bmatrix} = 0, \text{ and} \tag{1}$$

$$Bu + K\vartheta - J\ddot{\vartheta} + \begin{bmatrix} -LA^T S_\vartheta & LA^T C_\vartheta \end{bmatrix} \begin{bmatrix} h_x & h_y \end{bmatrix}^T = 0. \quad (2)$$

where A and B are the "addition" and "subtraction" operators [12]; $C_{\vartheta^k} = diag\left(\cos\vartheta^k\right), S_{\vartheta^k} = diag\left(\sin\vartheta^k\right)$, $K = -B\kappa B^{'}$, $\kappa = diag\left(\kappa_2, ..., \kappa_N\right)$, $B^{'} = \left(B^T\left(1,1\right) = 0\right)$.

Hence, internal force can be calculated as:

$$\begin{bmatrix} h_x & h_y \end{bmatrix}^T = \bar{B}\Omega_\vartheta \Gamma diags\left(V_\vartheta\right)V_\vartheta - \bar{B}m_l\left(-N_{1\vartheta}\ddot{\vartheta} + N_{2\vartheta}\dot{\vartheta}^2\right) \quad (3)$$

where $\bar{B} = \begin{bmatrix} B^1 & \\ & B^1 \end{bmatrix}, \Omega_{\vartheta^k} = \begin{bmatrix} C_{\vartheta^k} & -S_{\vartheta^k} \\ S_{\vartheta^k} & C_{\vartheta^k} \end{bmatrix}, N_{1\vartheta^k} = \begin{bmatrix} -F^k S_{\vartheta^k} \\ F^k C_{\vartheta^k} \end{bmatrix}, N_{2\vartheta^k} = \begin{bmatrix} F^k C_{\vartheta^k} \\ F^k S_{\vartheta^k} \end{bmatrix}$, $F^k = \left(B^T\right)^{-1} AL^k, L^k = diag\left(l^k\right)$, $V_{\vartheta^k} = -\Omega_{\vartheta^k}^T N_{1\vartheta^k}\dot{\vartheta}^k$, and $diags(*)$ is the signature matrix of $diag(*)$.

The thrust accumulated in the y direction is given by:

$$h_{y_1} = \bar{E}\Omega_\vartheta \Gamma diags\left(V_\vartheta\right)V_\vartheta - \bar{E}m\left(-N_{1\vartheta}\ddot{\vartheta} + N_{2\vartheta}\dot{\vartheta}^2\right),$$

where $\bar{E} = \begin{bmatrix} 0 & 1 \end{bmatrix} E^T, \Gamma^k = diag\left(s_t^k, s_n^k\right)$, $S_t^k = -0.5\rho c_l diag\left(s_t^k\right)$, $S_n^k = -0.5\rho c_l diag\left(s_n^k\right)$, c_l is the fluid coefficient of the propulsor, ρ is fluid density, and E is the distribution matrix [12].

Substituting the internal force (3) to the moment (2), leads to the propulsor locomotion model:

$$A_\vartheta \ddot{\vartheta} + K\vartheta + Bu + H_\vartheta = 0, \quad (4)$$

where $H_\vartheta = G_\vartheta \Omega_\vartheta \Gamma diags\left(V_\vartheta\right)V_\vartheta - G_\vartheta m N_{2\vartheta}\dot{\vartheta}^2$, and $A_{\vartheta^k} = -J^k + G_{\vartheta^k} m^k N_{1\vartheta^k}$, $G_{\vartheta^k} = \begin{bmatrix} -L^k A^T S_{\vartheta^k} & L^k A^T C_{\vartheta^k} \end{bmatrix}\bar{B}$.

2) Propulsor Flexural Rigidity Optimization

The propulsor flexural rigidity can be optimized by maximizing the thrust production given the same input torque. The optimization was formulated as:

$$\max_\kappa J\left(\vartheta, \kappa\right), \quad where \;\; J\left(\vartheta, \kappa\right) = \int_0^\tau h_{y_1}\left(\ddot{\vartheta}, \dot{\vartheta}, \vartheta\right)dt. \quad (5)$$

$$\text{Subjected to} \quad \begin{aligned} & h_l = A_\vartheta \ddot{\vartheta} + K\vartheta + Bu + H_\vartheta = 0, \\ & g_0 = \vartheta\left(0, \kappa\right) = 0.87, \text{ and} \\ & g_1 = \dot{\vartheta}\left(0, \kappa\right) = 0, \end{aligned} \quad (6)$$

where g_0 and g_1 are initial conditions for the propulsor orientation and angular velocity respectively.

In order to maximize $J\left(\vartheta, \kappa\right)$, the gradient descent method was used and solved via the adjoint method [13]. The Lagrangian term for the optimization is:

$$L\left(\vartheta, \kappa\right) = \int_0^\tau \left(h_{y_1} + \lambda_1^T h_l\right)dt + \lambda_2^T g_0 + \lambda_3^T g_1 \quad (7)$$

By applying the adjoint method, the total derivative of $J\left(\vartheta, \kappa\right)$ can be derived as:

$$\nabla_\kappa J\left(\vartheta, \kappa\right) = d_\kappa L\left(\vartheta, \kappa\right) = \int_0^\tau \left(\partial_\kappa h_{y_1} + \lambda_1^T \partial_\kappa h_l\right)dt \quad (8)$$

The conditions used to calculate $\nabla_\kappa J\left(\vartheta, \kappa\right)$ are:

$$\ddot{\lambda}_1^T = -\left(\partial_\vartheta h_{y_1} + \lambda_1^T \partial_\vartheta h_l - \dot{\lambda}_1^T \partial_{\dot{\vartheta}} h_l\right)\left(\partial_{\ddot{\vartheta}} h_l\right)^{-1}, \quad (9)$$

$$\lambda_1^T\left(\tau\right) = -\partial_{\ddot{\vartheta}} h_{y_1}\left(\partial_{\ddot{\vartheta}} h_l\right)^{-1}\big|_\tau, \text{ and} \quad (10)$$

$$\dot{\lambda}_1^T\left(\tau\right) = \left(\partial_{\dot{\vartheta}} h_{y_1} + \lambda_1^T \partial_{\dot{\vartheta}} h_l\right)\left(\partial_{\ddot{\vartheta}} h_l\right)^{-1}\big|_\tau. \quad (11)$$

The algorithm for the optimal flexural rigidity κ calculation is given in Fig.4.

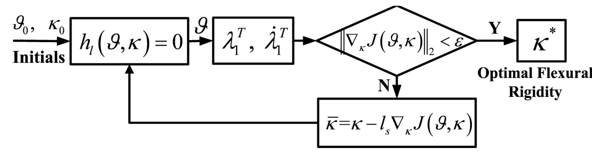

Fig.4 Flow chart to optimize the flexural rigidity

B. Beating Pattern Optimization

1) Dynamics Model for the Whirligig Beetle Robot

(1) Body Model

In the global frame, using the resistive force theory, the robot body locomotion was modeled by balancing moment and force applied by the fluid and propulsors (Fig.3(b)).

$$\sum_{k=1}^4 \begin{bmatrix} h_{y_1}^k & h_{y_1}^k \end{bmatrix} - M_b\ddot{\Phi} + R_b diag\left(c_{bl}, c_{bn}\right) diags\left(R_b^T\dot{\Phi}\right)R_b^T\dot{\Phi} = 0, \text{and} \quad (12)$$

$$\sum_{k=1}^4 \left(e_b r_b^k\right)^T R_b^T \begin{bmatrix} h_{x_1}^k & h_{y_1}^k \end{bmatrix}^T + \sum_{k=1}^4 u_1^k - J_b\ddot{\theta}_b - c_{bo}\ddot{\theta}_b = 0. \quad (13)$$

where $c_{bl} = -0.5\sigma S_l c_b$, $c_{bn} = -0.5\sigma S_n c_b$, c_b is the fluid drag coefficient, S_l, S_n are the projection areas in the longitude and normal direction of the robot body; c_{bo} is fluid rotational coefficient for the robot body; $R_b = \begin{bmatrix} \cos\theta_b & -\sin\theta_b \\ \sin\theta_b & \cos\theta_b \end{bmatrix}$, $e_b = \begin{bmatrix} 0 & -1 \\ 1 & 0 \end{bmatrix}$.

(2) Multiple Propulsor Model

Similar to the model for the isolated propulsor in *Section III-A*, the model for the propulsor mounted on the swimming robot can be derived as:

$$\begin{bmatrix} f_x^k \\ f_y^k \end{bmatrix} - m^k \begin{bmatrix} \ddot{x}^k \\ \ddot{y}^k \end{bmatrix} + \begin{bmatrix} B & \\ & B \end{bmatrix}\begin{bmatrix} h_x^k \\ h_y^k \end{bmatrix} = 0, \quad (14)$$

$$Bu^k + K^k\vartheta^k - J^k\ddot{\vartheta}^k + \begin{bmatrix} -LA^T S_{\vartheta^k} & LA^T C_{\vartheta^k} \end{bmatrix}\begin{bmatrix} h_x^k & h_y^k \end{bmatrix}^T = 0. \quad (15)$$

The internal force on the k-th propulsor is:

$$\begin{bmatrix} h_x^k & h_y^k \end{bmatrix}^T = -\bar{B}m^k E\ddot{\Phi} - \bar{B}m^k ER_b e_b r_b^k \ddot{\theta}_b + \bar{B}m^k N_{1\vartheta^k}\ddot{\vartheta}^k + \bar{B}\bar{H}_{\vartheta^k}. \quad (16)$$

Total thrust produced by the k-th propulsor is:

$$\begin{bmatrix} h_{x_1}^k & h_{y_1}^k \end{bmatrix}^T = E^T\left(-m^k E\ddot{\Phi} - m^k ER_b e_b r_b^k \ddot{\theta}_b + m^k N_{1\vartheta^k}\ddot{\vartheta}^k\right) + H_{\vartheta^k}, \quad (17)$$

where $\bar{H}_{\vartheta_1^k} := E^T \bar{H}_{\vartheta^k}, \bar{H}_{\vartheta^k} := m^k \left(E R_b r_b^k \dot{\theta}_b^2 - N_{2\vartheta^k} \dot{\vartheta}^{k2} \right) + \left[f_x^k \quad f_y^k \right]^T$.

(3) Integrated Model for the Whirligig Beetle Robot

With the body and the k-th propulsor model derived in the *SectionⅢ-B(1) and (2),* an integrated dynamics model for the whirligig beetle robot can be derived. The integrated model for the k-th propulsor can be obtained by substituting the internal force (16) to (15):

$$A_{1\vartheta^k} \ddot{\vartheta}^k + A_{2\vartheta^k} \ddot{\theta}_b + A_{3\vartheta^k} \ddot{\Phi}_b = -Bu^k - K^k \vartheta^k - G_{\vartheta^k} \bar{H}_{\vartheta^k}. \quad (18)$$

By substituting thrust from each propulsor (17) to the body model, we obtain the integrated model for the body:

$$\sum_{k=1}^{4} A_{11\vartheta^k} \ddot{\vartheta}^k + A_{12\vartheta} \ddot{\theta}_b + A_{13\vartheta} \ddot{\Phi}_b = -B_{11}, \quad (19)$$

$$\sum_{k=1}^{4} A_{21\vartheta^k} \ddot{\vartheta}^k + A_{22\vartheta} \ddot{\theta}_b + A_{23\vartheta} \ddot{\Phi}_b = -B_{21} - \sum_{k=1}^{4} u_1^k, \quad (20)$$

where the coefficients matrices are:

$$A_{11\vartheta^k} = E^T m^k N_{1\vartheta^k},\ A_{12\vartheta} = -\sum_{k=1}^{4} E^T m^k E R_b e_b r_b^k,$$

$$A_{13\vartheta} = \text{-}diag\left(M_b, M_b\right) \text{-} \sum_{k=1}^{4} E^T m^k E, A_{21\vartheta^k} := \left(e_b r_b^k\right)^T R_b^T E^T m^j N_{1\vartheta^k},$$

$$A_{22\vartheta} = \text{-}J_b \text{-} \sum_{k=1}^{4} \left(E R_b e_b r_b^k\right)^T m^k E R_b e_b r_b^k,\ A_{23\vartheta} = -\sum_{k=1}^{4} \left(E R_b e_b r_b^k\right)^T m^k E,$$

$$B_{11} = \sum_{K=1}^{4} H_{1\vartheta^k} + R_b diag\left(c_{b_l}, c_{b_n}\right) diags\left(R_b^T \dot{\Phi}_b\right) R_b^T \dot{\Phi}_b,$$

$$B_{21\vartheta} = \sum_{k=1}^{4} \left(e_b r_b^k\right)^T R_b^T H_{1\vartheta^k} - c_{bo} \dot{\theta}_b, A_{1\vartheta^k} = G_{\vartheta^k} m^k N_{1\vartheta^k} - J^k,$$

$$A_{2\vartheta^k} = -G_{\vartheta^k} m^k E R_b e_b r_b^k,\ A_{3\vartheta^k} = -G_{\vartheta^k} m^j E, K^k = B \kappa^k B' \vartheta^k.$$

2) Beating Pattern Optimization

(1) Optimization Problem Formulation

To implement the beating pattern optimization, we redefined the swimming robot model (18) (19) and (20) in the control format:

$$\ddot{X} = g\left(\dot{X}, X\right) + h\left(\dot{X}, X\right) u, \quad (21)$$

where $X = \left[\vartheta^1 \quad \ldots \quad \vartheta^4 \quad \theta_b \quad \Phi_b\right]^T$ is state variable vector; $g\left(\dot{X}, X\right) = \bar{A}\left(X\right) B\left(X\right)$, $h\left(\dot{X}, X\right) = \bar{A}\left(X\right) C\left(X\right)$, and

$$\bar{A}(X) = \begin{bmatrix} A_{11\vartheta^1} & \cdots & A_{11\vartheta^4} & A_{12\vartheta} & A_{13\vartheta} \\ A_{21\vartheta^1} & \cdots & A_{21\vartheta^4} & A_{22\vartheta} & A_{23\vartheta} \\ A_{1\vartheta^1} & & & A_{2\vartheta^1} & A_{3\vartheta^1} \\ & \cdots & & \cdots & \cdots \\ & & A_{1\vartheta^4} & A_{2\vartheta^4} & A_{3\vartheta^4} \end{bmatrix}^{-1}, B(X) = -\begin{bmatrix} B_{11} \\ B_{21} \\ K^1 \vartheta^1 + G^1 \bar{H}_{\vartheta^1} \\ \cdots \\ K^4 \vartheta^4 + G^4 \bar{H}_{\vartheta^4} \end{bmatrix}, C(X) = -\begin{bmatrix} 0 \\ \sum_{k=1}^{4} u_1^k \\ Bu^1 \\ \cdots \\ Bu^4 \end{bmatrix}.$$

Since propulsion efficiency is closely related to the distance travelled, energy consumption, and propulsor states, the optimization problem can be formulated as minimization of energy over a predefined travelling distance, and propulsor states errors to disallow out-of-bounds propulsor orientations. Energy consumption from t_0 to t_f can be calculated as $J_u = \int_{t_0}^{t_f} u u^T dt$. States constraints for propulsor orientation are:

$$\begin{cases} C_{1,1}\left(X\right) = -4.01 - X_1\left(t\right) \le 0 \\ C_{2,1}\left(X\right) = X_1\left(t\right) + \pi/2 \le 0 \end{cases}, \quad \begin{cases} C_{1,1+N}\left(X\right) = -\pi/2 - X_{1+N} \le 0 \\ C_{2,1+N}\left(X\right) = X_{1+N}\left(t\right) - 0.87 \le 0 \end{cases}, \quad (22)$$
$$\begin{cases} C_{3,1+2N}\left(X\right) = -4.01 - X_{1+2N}\left(t\right) \le 0 \\ C_{3,1+2N}\left(X\right) = X_{1+2N}\left(t\right) + \pi/2 \le 0 \end{cases}, \begin{cases} C_{4,1+3N}\left(X\right) = -\pi/2 - X_{1+3N}\left(t\right) \le 0 \\ C_{4,1+3N}\left(X\right) = X_{1+3N}\left(t\right) - 0.87 \le 0 \end{cases}.$$

By setting $C_i^+ = \max\left(0, C_{1,i}\left(X\right)\right) + \max\left(0, C_{2,i}\left(X\right)\right), C_{2,i}{}^+\left(X\right)$,

The constraints become $\gamma\left(X\right) = \left[C_1^+ \quad \ldots \quad C_{N+3}^+\right]^T$.

Hence, the cost function can be written as:

$$J_{us} = J_u + \int_{t_0}^{t_f} \gamma\left(X\right) dt \quad (23)$$

The beating pattern optimization is formulated as:

$$\min_u J_{us}, \text{ subject to } \ddot{X} = g\left(\dot{X}, X\right) + h\left(\dot{X}, X\right) u. \quad (24)$$

The boundary conditions are:

$$X\left(t_0\right) = 0,\ \dot{X}\left(t_0\right) = 0,\ X_1\left(t_f\right) = \bar{x}_b,\ X_2\left(t_f\right) = \bar{y}_b. \quad (25)$$

(2) Optimization Method

By redefining $v = \dot{X}$, the robot's model (21) becomes:

$$\dot{X} = v, \text{ and } \dot{v} = g\left(v, X\right) + h\left(v, X\right) u. \quad (26)$$

The Hamilton equation for the optimization is:

$$H = u^T u + \gamma\left(X\right) + \lambda_v^T \left(g\left(v, X\right) + h\left(v, X\right) u\right) + \lambda_X^T v. \quad (27)$$

By applying the Pontryagin's Maximum Principle, the necessary conditions for minimizing the energy consumption and states errors are obtained as:

$$\dot{\lambda}_X^*(t) = -\left(\frac{\partial g(v, X)}{\partial X}\right)^T \lambda_v - u^T \left(\frac{\partial h(v, X)}{\partial X}\right)^T \lambda_v - \frac{\partial \gamma(X)}{\partial X}, \quad (28)$$

$$\dot{\lambda}_v^*(t) = -\left(\frac{\partial g(v, X)}{\partial v}\right)^T \lambda_v - u^T \left(\frac{\partial h(v, X)}{\partial v}\right)^T \lambda_v - \lambda_X, \text{ and} \quad (29)$$

$$\frac{\partial H}{\partial u} = 2u^T + \lambda_v{}^T h\left(v, X\right) = 0. \quad (30)$$

The optimal beating pattern can be obtained by solving the boundary value problem (26) (28) and (29), with the boundary conditions (25). This optimization problem can be solved using the bvp5c solver provided by MATLAB [14].

Ⅳ. RESULTS AND DISCUSSION

In order to validate the proposed optimization methods, we tested the swimming robot using the results from simulations and experiments. Parameters used in the simulations and experiments are listed in Tab.1.

TABLE1 PARAMETERS USED IN WHIRLIGIG BEETLE INSPIRED ROBOT SIMULATION

Parameter	Notation	Value	Parameter	Notation	Value
body mass	M_b	0.8167kg	propulsor length	L	0.10m
body rotational coefficient	c_{bo}	1	link moment of inertia	J_i^k	7.33×10^{-3} kg·m^2
body moment of inertia	J_b	2.86×10^{-3} kg·m^2	propulsor drag coefficient	c_l	2.3
body translation coefficient	c_b	0.39	propulsor link number	N	6
motor position	(r_x, r_y)	29mm×22mm	link mass	m_i^k	0.127kg
body half axis	$a\times b\times c$	93mm×47mm×28mm	propulsor width	W	0.07m
fluid density	ρ	1000kg/m^3	propulsor number	k	4

A. Compliant Propulsor Flexural Rigidity Optimization

Through flexural rigidity optimization, we found that stiff ends and soft middle on the recovery stroke side (Fig.5 (a)) allowed the propulsor to achieve larger thrust.

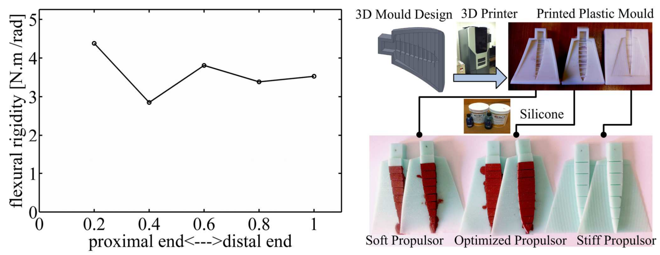

(a) (b)

Fig.5 Flexural rigidity optimization (a) and propulsor fabrication (b). With the selected silicone (Young's Modulus is 1.31×105 Pa for mint green silicone, and 2.78×105 Pa for red silicone), the mould was designed based on the optimized propulsor using 3D drawing software (Solidworks 2012). The mould was fabricated by STRATASYS FORTUS 250mc 3D printer.

To validate the optimized flexural rigidity, the swimming robot was tested with an arbitrary selected flexural rigidity (70% of the optimized value) for the propulsors. The results in Fig.6 indicated that the optimized propulsor achieved a larger acceleration when compared to the arbitrary propulsor, especially during the recovery stroke (i.e., 0.8s~1.50s).

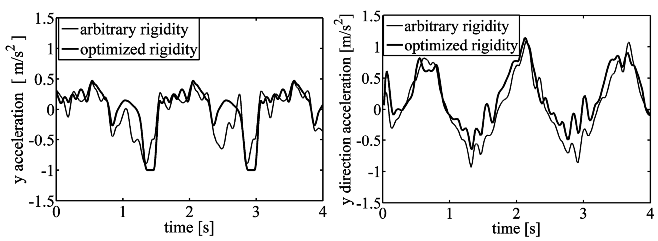

(a) (b)

Fig.6 (a) *Y* direction acceleration from simulation and (b) experiment.

B. Beating Pattern Optimization

1) Propulsor Beating Sequence

Using the optimization method proposed in *Section III-B*, the efficient beating pattern (Fig.7 (a)) was identified. Fig.7 (b) shows that the robot makes a sinusoidal-like oscillation when propelled by the optimized beating pattern. The three swimming periods in Fig.7 (c) accurately correspond to the optimized beating pattern, further illustrating that alternating beating of propulsors improves the propulsion efficiency.

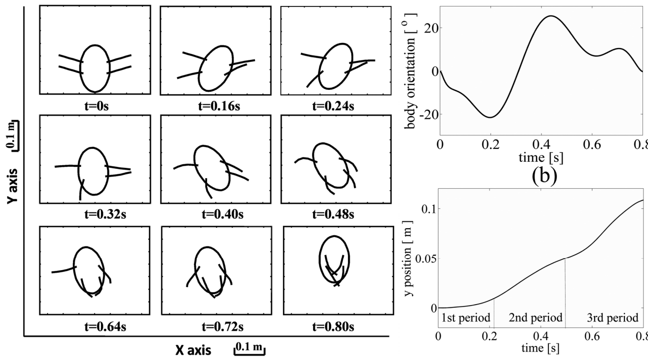

(a) (c)

Fig. 7 (a) Optimized beating pattern; (b) Body orientation; (c) Three swimming periods.

2) Optimal Beating Pattern For the Robot

It was difficult to test the robot with the optimized torque due to the actuation limitations from the servos. The experimental torque was obtained for the robot tested by guaranteeing the robot propulsors following the optimized beating pattern. The body orientation in Fig.8 (a) and (b) showed that the robot only rotated during the power stroke (i.e., 0s-0.8s) and kept the same posture during the recovery stroke (i.e., 0.8s-1.5s). This helped the robot maintain a stable motion for high speed coasting.

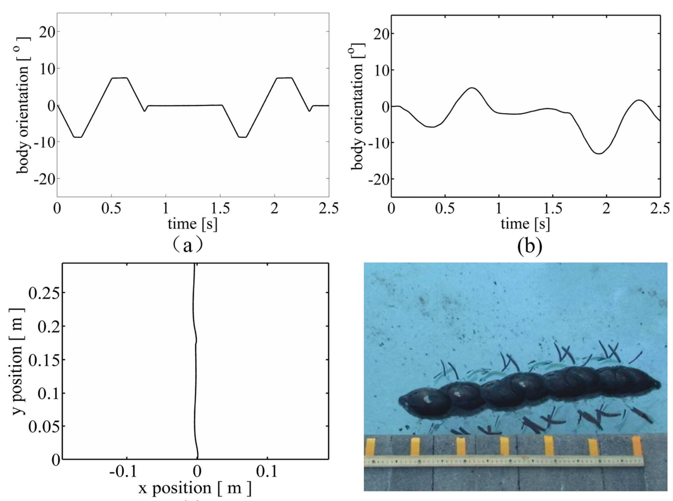

(c) (d)

Fig.8 (a) Simulated and experimental (b) robot body orientation; (c) simulated and experimental (d) robot trajectory.

Fig.8 (c) and (d) show that propelled by the optimized beating pattern, the robot made a small *S*-shape path while swimming, with a speed of 0.11m/s. Similar locomotion habits have been observed for whirligig beetles.

3) Beating Pattern Comparison

In order to validate the efficiency of the optimized beating pattern, three groups of tests were conducted, including 1) simultaneous beating of four propulsors (*hr*+*hl*+*mr*+*ml*), 2) alternating, symmetric beating of the hind and middle propulsors (*hr*+*hl*→*mr*+*ml*), and 3) the optimized asymmetric, alternating beating pattern (*hl*→*mr*+*hr*→*ml*). Both the travelling distance (Fig.9) and efficiency comparisons (Tab.2) indicated that the optimized asymmetric, alternating beating was the most efficient.

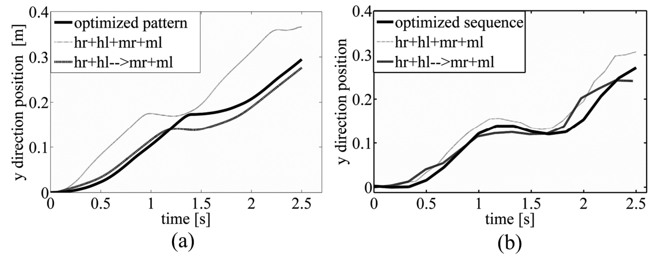

Fig. 9 Simulated and experimental travelling distance in the *y* direction for the three beating patterns. Trajectories were extracted using image processing method by recognizing feature points [15].

Comparing the optimized pattern to the other cases further illustrates how the beating pattern can be adjusted to improve the propulsion efficiency. First, as compared to the *hr+hl+mr+ml* pattern, we noticed the alternating propulsor beating helps to increase the propulsion ability, and the efficiency was lifted from 0.18/***0.18*** to 0.35/***0.20*** after implementing the optimized pattern. Second, the comparison to the *hr+hl→mr+ml* pattern indicated that asymmetric beating contributes to the swimming efficiency, as shown by the symmetric beating of different side propulsors being 33%/***15%*** less than the efficiency created by the asymmetric beating, where the Common/***Bolded, Italic*** font formats represent the simulation/***experimental*** data respectively.

TABLE 2. PROPULSION EFFICIENCY COMPARISONS

Beating Pattern	Distance (*L*) Unit: *meter*		Energy (*En*) Unit: *J*		Efficiency (*L/En*)		Normalized Efficiency	
hr + hl + mr + ml	0.36	***0.30±0.016***	1.92	***1.65±0.040***	0.18	***0.18***	0.55	***0.90***
hr + hl → mr + ml	0.27	***0.25±0.008***	1.12	***1.44±0.033***	0.23	***0.17***	0.67	***0.85***
Optimized Pattern	0.29	***0.28±0.019***	0.85	***1.40±0.028***	0.35	***0.20***	1.00	***1.00***

Furthermore, it can be seen that only the optimized beating pattern causes the sinusoidal-like oscillation, and *S*-shaped trajectory. This confirmed the observation from our previous study that the *S*-shaped swimming is more energy efficient for the whirligig beetle [5].

Ⅴ. CONCLUSION

In this paper, we have developed a bio-inspired energy efficient propulsion mechanism, and validated the design using a whirligig beetle inspired swimming robot. Using the optimized flexural rigidity and beating pattern, the whirligig beetle inspired swimming robot has demonstrated all key features observed in whirligig beetles, such as extending the surface area during the power stroke, alternating asymmetric beating, and oscillation of the body orientation to generate the *S*-shaped trajectory.

REFERENCE

[1] M. Karpelson, J. P. Whitney, W. Gu-Yeon, and R. J. Wood, "Design and fabrication of ultralight high-voltage power circuits for flapping-wing robotic insects," in *in Proc. 26th IEEE APEC*, Mar. 2011, pp. 2070-2077.

[2] G. Lauder and P. A. Madden, "Learning from fish: Kinematics and experimental hydrodynamics for roboticists," *Int. J. Autom. Comput.,* vol. 3, pp. 325-335, Oct. 2006.

[3] W. Liu, X. Jia, F. Wang, and Z. Jia, "An in-pipe wireless swimming microrobot driven by giant magnetostrictive thin film," *Sens. Actuators, A,* vol. 160, pp. 101-108, 2010.

[4] W. Nachtigall, "Funktionelle Morphologie, Kinematik und Hydromechanik des Ruderapparates von. Gyrinus.," *Z. Vergl. Physiol.,* vol. 45, pp. 193-226, 1961.

[5] Z. Xu, S. C. Lenaghan, B. E. Reese, X. Jia, and M. Zhang, "Experimental Studies and Dynamics Modeling Analysis of the Swimming and Diving of Whirligig Beetles (Coleoptera:Gyrinidae)," *PLoS Comput. Biol.,* vol. 8, p. e1002792, 2012.

[6] F. E. Fish and A. J. Nicastro, "Aquatic turning performance by the whirligig beetle: constraints on maneuverability by a rigid biological system," *J. Exp. Biol.,* vol. 206, pp. 1649-1656, May 15, 2003.

[7] J. Voise and J. Casas, "The management of fluid and wave resistances by whirligig beetles," *J. Royal Soc. Interface,* vol. 7, pp. 343-352, 2010.

[8] W. Nachtigall, "Locomotion: mechanics and hydrodynamics of swimming in aquatic insects," in *The physiology of Insecta*. vol. III, M. Rockstein, Ed., ed, New York: Academic, 1974, pp. 381–432.

[9] F. Closa, A. D. Chepelianskii, and E. Raphael, "Capillary-gravity waves generated by a sudden object motion," *Physics of Fluids,* vol. 22, May 2010.

[10] X. Gao and L. Jiang, "Biophysics: Water-repellent legs of water striders," *Nature,* vol. 432, pp. 36-36, 2004.

[11] K. Suzumori, S. Endo, T. Kanda, N. Kato, and H. Suzuki, "A bending pneumatic rubber actuator realizing soft-bodied manta swimming robot," in *Proc. IEEE Int. Conf. Rob. Autom.*, 2007, pp. 4975-4980.

[12] X. Jia, X. Li, S. Lenaghan, M. Zhang, "Design of Efficient Propulsion for Nanorobots," *IEEE Trans. Robot.,* Accepted For Publication.

[13] A. Jameson, "Aerodynamic design via control theory," *J. Sci. Comput.,* vol. 3, pp. 233-260, 1988.

[14] L. F. Shampine, J. Kierzenka, and M. W. Reichelt. Solving boundary value problems for ordinary differential equations in MATLAB with bvp4c [Online]. Available: http://www.mathworks.com/bvp_tutorial

[15] W. Liu, X. Jia, Z. Jia, S. Liu, B. Wang, and J. Du, "Fast dimensional measurement method and experiment of the forgings under high temperature," *J. Mater. Process. Technol.,* vol. 211, pp. 237-244, 2011.